Scilight

Nanoenergy Communications

https://www.sciltp.com/journals/nc

Article

Piezoelectric Paper Energy Harvesters Based on Microwave-Assisted Grown ZnO Rods

Maria Morais [1], Tiago Silva [1], Andreia dos Santos [2], Margarida António [1], Jorge Martins [1], Cristina Gaspar [2], Elvira Fortunato [1], Rodrigo Martins [1], Luís Pereira [1,2], Pedro Barquinha [1] and Ana Rovisco [1,*]

[1] CENIMAT|i3N, Department of Materials Science, School of Science and Technology, NOVA University Lisbon and CEMOP/UNINOVA, 2829-516 Caparica, Portugal

[2] ALMASCIENCE—Investigação e Desenvolvimento em Celulose para Aplicações Inteligentes e Sustentáveis, Campus da Caparica, 2829-516 Caparica, Portugal

* Correspondence: a.rovisco@fct.unl.pt

How To Cite: Morais, M.; Silva, T.; Santos, A.D.; et al. Piezoelectric Paper Energy Harvesters Based on Microwave-Assisted Grown ZnO Rods. *Nanoenergy Communications* **2026**, *1*(1), 6. https://doi.org/10.53941/nc.2026.100006

Received: 7 January 2026
Revised: 12 March 2026
Accepted: 20 March 2026
Published: 31 March 2026

Abstract: The growing energy demand, combined with the rising volume of e-waste, demands an urgent search for sustainable energy-harvesting devices. Among the several energy sources, mechanical energy is the most explored due to its abundance. In this context, piezoelectric energy harvesters have great potential, as they leverage the synergy between tribo- and piezoelectric effects to convert mechanical into electrical energy with high efficiency. Herein, the potential of sustainable materials to produce paper-based energy harvesters is explored. Specifically, paper is used as both active layer and substrate and the response of devices based on this material in different forms (pristine, embedded with matrices of cellulose derivatives and embedded with composites of hydrothermally synthesized one-dimensional zinc oxide—ZnO—particles and polymeric matrices) is evaluated. Different architectures were studied, namely the active layer sandwiched between two commercial electrodes and devices based on paper substrates with screen-printed silver electrodes. Among these, a maximum output of (3.5 ± 0.8) V was obtained with devices based on Whatman paper embedded with ZnO/ethylcellulose nanocomposites sandwiched between commercial electrodes, and the same active layer with screen-printed electrodes yielded an output voltage of (0.29 ± 0.01) V, for an impact force of 10 N. The present results thus represent a promising avenue for the development of sustainable devices, paving the way for eco-friendly, cost-effective and versatile energy-harvesting technologies.

Keywords: energy harvesting; piezoelectricity; triboelectricity; zinc oxide; paper; cellulose

1. Introduction

The current environmental scenario demands an urgent search for more sustainable energy sources [1,2]. Moreover, the need to develop green alternatives to obtain electrical energy has become vital due to the growing energy demand [3,4]. Nowadays, devices such as mobile electronics, sensors and implantable biomedical devices are powered by batteries that often present a shorter lifetime than the device and whose replacement can be difficult and inconvenient [5,6]. As such, the focus has shifted to developing devices that can harvest energy from different sources, such as heat, electromagnetic radiation, mechanical vibrations and fluid flows, then redistributing it to the final application, such as powering devices [7,8]. Among the several ambient energy sources, mechanical energy is the most ubiquitous and versatile since it can be harvested from different sources such as vibration, flow and

motion [9,10]. Among these, biomechanical motion can generate power in the order of 67 W [11]. Within this framework, several alternatives have been explored to convert mechanical energy into usable electrical energy.

Two approaches to harvesting surrounding mechanical energy are the use of triboelectric and piezoelectric energy harvesters, which absorb and convert mechanical into electrical energy [8,12]. The working mechanism of triboelectric devices relies on the coupling of the triboelectric effect (also known as contact electrification) with electrostatic induction to convert mechanical stimuli into electrical signals [13,14]. In these devices, when two different materials contact each other, the material with the greater electron-attracting ability becomes negatively charged, and the other becomes positively charged [15,16]. The generated charges are non-mobile and have a long lifetime. Upon physical separation, the charges in the interfacial region will separate, creating a potential difference and causing electrons to flow in the external circuit to cancel this difference [11,15]. Triboelectric harvesters have four working modes depending on the relative motion of the materials: single-electrode, contact-separation, free-standing triboelectric layer and lateral sliding [16,17]. By comparison, piezoelectric energy harvesting relies on an alternative electromechanical conversion principle.

Piezoelectric harvesters are based on the displacement of dipoles within the active material due to the absence of a center of symmetry within its structure [15,18,19]. As such, piezoelectric devices do not require contact with other materials, contrary to triboelectric ones [9]. Besides being durable and more sensitive to minor strains, piezoelectric harvesters can be manufactured in various dimensions and compact structures, which can be incorporated into different circuits. Therefore, piezoelectricity is a promising approach for developing harvesters that have been applied to wireless electronics, implantable biomedical devices and transportation [6,19]. Generally, piezoelectric materials fall into two groups: organic and inorganic materials [18,20]. Polyvinylidene fluoride (PVDF) and poly(vinylidene fluoride-co-trifluoroethylene) (P(VDF-TrFE)) are the most well-known organic piezoelectric materials, exhibiting piezoelectric coefficients around −33 $pC \cdot N^{-1}$ [18,21]. The piezoelectric behavior of these polymers originates from the asymmetric distribution of hydrogen and fluorine atoms in the β-phase [2,22]. However, achieving optimal piezoelectricity in PVDF-based materials often requires post-production processes, such as poling, which involve high temperatures and add complexity to the fabrication process [23].

When compared with organic piezoelectric materials, inorganic materials present higher piezoelectric constants [24,25]. Their extensive use in energy harvesters stems from their sensitivity to mechanical deformations such as bending, stretching, twisting and pressing [9]. The group of inorganic materials includes ceramics (e.g., lead zirconate titanate—PZT), as well as nanostructured films and particles [22,25]. The piezoelectric response of these materials is based on the deformation of their crystal lattice [22,26]. Generally, inorganic piezoelectric materials exhibit either a wurtzite or a perovskite crystal structure [9]. Among these, materials with wurtzite structure, including cadmium sulfide (CdS), gallium nitride (GaN), indium nitride (InN), aluminum nitride (AlN), zinc oxide (ZnO) and zinc sulfide (ZnS), have garnered significant attention due to their excellent mechanical properties and high stability [24,27]. Among the wurtzite-structured materials, ZnO has been widely explored. Unlike PZT, which despite its high piezoelectric coefficient (d_{33} between 500 and 600 $pC \cdot N^{-1}$ [28] against 10 to 12 $pC \cdot N^{-1}$ for ZnO [29]) poses environmental and health risks due to its lead content [28], ZnO is environmentally benign, non-toxic and biodegradable [30–33]. Additionally, ZnO avoids the need for high-temperature processing or poling, unlike PVDF derivatives [23], making it a scalable and sustainable choice. This metal oxide can be easily synthesized with different properties through cost-effective, low-temperature and straightforward approaches, and its high thermal and chemical stability, antimicrobial properties and versatility explain its widespread use in optoelectronics, sensors, photocatalysis and piezoelectric devices [34–38]. However, translating the favorable properties of ZnO into flexible devices requires suitable substrate materials.

Owing to their properties such as cost-effectiveness, abundance, lightness, flexibility, non-toxicity, and environmental friendliness, paper substrates have been one of the main research topics in the field of flexible electronics [39–43]. The development of triboelectric energy harvesters that include paper in their structure has already been reported [4,44–46]. For the development of triboelectric harvesters, paper acts as an active layer and conductive materials are deposited on each side to serve as an electrode [45]. In the case of paper-based piezoelectric sensors, paper is functionalized with an active material, such as nanostructures [45]. Although several reports of paper-based harvesters already exist, there is still much room to improve their performance or simplify the production process [45,46]. In this context, the active layer plays a fundamental role in determining device performance, with polymeric materials constituting a key component. Among the nature-derived and synthetic polymers explored for energy harvesting applications, cellulose has attracted significant interest.

Cellulose stands out among the bio-derived polymers due to its abundance, non-toxicity and cost-effectiveness. This biodegradable polymer has a piezoelectric coefficient between 26 and 60 $pC \cdot N^{-1}$ [13,47], and its use for the development of nanogenerators has already been reported [15,48–50]. To further enhance and tailor these properties, efforts have been directed toward designing composite materials.

Nanocomposites, i.e., composites of dielectric materials and nanostructures, offer the possibility to tailor specific properties of the final material, such as mechanical strength, dielectric constant and surface roughness [51,52], simultaneously protecting the piezoelectric structures, which typically have a brittle and fragile nature. As such, this work explores the potential of sustainable materials to produce nanocomposite-based energy harvesters. More specifically, harvesters in which paper substrates serve as both the active layer and the substrate for electrode material deposition were developed to replace commonly used, environmentally taxing materials such as polydimethylsiloxane (PDMS) and indium tin oxide-coated polyethylene terephthalate (PET/ITO) substrates. Alongside the produced harvesters based on paper substrates with embedded cellulose derivatives, devices based on nanocomposites of cellulose derivatives and ZnO were also produced, taking advantage of the intrinsic piezoelectricity of the nanostructures of this metal oxide. The performance of each architecture was evaluated, with a maximum output voltage of (3.5 ± 0.8) V obtained for devices based on Whatman paper embedded with ZnO@ethylcellulose nanocomposites under an impact force of 10 N. The same active layer sandwiched between screen-printed electrodes yielded a maximum output voltage of (0.29 ± 0.01) V. The presented results demonstrate the feasibility of using sustainable materials and processes to produce energy harvesters, paving the way for the development of eco-friendly, cost-effective energy-harvesting technologies with potential applications across fields such as healthcare, environmental monitoring and wireless sensing. In sum, this work demonstrates a distinctive and practical approach to developing cellulose-based energy harvesters by combining microwave-assisted hydrothermal synthesis of ZnO particles with coating and printing techniques. The reported approach not only reduces processing complexity but also explicitly shifts away from unsustainable materials, while exploiting the structural versatility of ZnO nanostructures, to enable systematic tuning of device performance through active layer composition and device design.

2. Materials and Methods

2.1. Microwave-Assisted Hydrothermal Synthesis of ZnO Nanorods

The ZnO nanorods were obtained by hydrothermal synthesis assisted by microwave irradiation, following an already reported procedure [53]. Zinc acetate dihydrate ($C_4H_{10}O_6Zn$, 98–101%, CAS: 5970-45-6) from Thermo Scientific Chemicals (Waltham, MA, USA) and sodium hydroxide (NaOH, ≥98%, CAS: 1310-73-2) from Labkem (Barcelona, Spain) were the precursors used for the synthesis of the metal oxide nanostructures. Additionally, sodium dodecyl sulfate ($NaC_{12}H_{25}SO_4$, 95%, CAS: 151-21-3) from Scharlau (Barcelona, Spain) was the chosen surfactant. The synthesis was carried out in a solvent mixture of deionized water and 2-ethoxyethanol ($C_4H_{10}O_2$, 99%, CAS: 110-80-5) from Honeywell Research Chemicals (Charlotte, NC, USA). Briefly, 3.3 g of zinc acetate dihydrate was dissolved in 30 mL of deionized water under magnetic stirring. Subsequently, 9.6 g of sodium hydroxide was added to the zinc solution, and the mixture was stirred continuously until a homogeneous mixture was obtained. In parallel, a surfactant solution was prepared by dissolving 0.045 g of sodium dodecyl sulfate in 150 mL of deionized water. Once both solutions were completely dissolved, 6 mL of the zinc precursor solution, 15 mL of the surfactant solution and 30 mL of 2-ethoxyethanol were combined and stirred for 5 min. The final mixture was evenly distributed by three Teflon® vessels, each containing 17 mL of the prepared solution. These vessels were transferred to a microwave digestion system (CEM-MarsOne, CEM, Matthews, NC, USA) and heated at 110 °C for 40 min, under a power of 600 W. After completion of the reaction, the vessels were allowed to cool down to room temperature and the synthesized ZnO structures were cleaned by centrifugation at 3000 rpm for 3 min using deionized water and isopropanol, alternating solvents after each cycle. Finally, the produced particles were dried under vacuum in a desiccator (VACUO-TEMP, J. P. Selecta, Barcelona, Spain) at 85 °C for 5 h.

2.2. Preparation of Polymer Matrices and ZnO@polymer Nanocomposites

The polymers used to produce the active layer of the energy harvesting devices (EHDs) were polydimethylsiloxane (PDMS), which is composed of two parts: elastomer (Dow Corning, Michigan, USA) and curing agent (Sylgard 184, Dow Corning, Freeland, MI, USA), and the cellulose derivatives sodium carboxymethyl cellulose ($C_8H_{15}NaO_8$, average Mw ~ 250,000, degree of substitution 0.7, CAS: 9004-32-4) and ethylcellulose ($C_{20}H_{38}O_{11}$, extent of labeling: 48% ethoxyl, CAS: 9004-57-3) from Sigma-Aldrich (Massachusetts, USA) hereafter referred to as CMC and EC. EC was dissolved in a mixture of 4-hydroxy-4-methyl-2-pentanone ($C_6H_{12}O_2$; 99%; CAS: 123-42-2) from Sigma-Aldrich (Burlington, MA, USA) and absolute ethanol (C_2H_5OH; ≥99.9%; CAS: 64-17-5) from Carlo Erba (Emmendingen, Germany). For the production of the PDMS-based devices, PDMS was prepared according to a procedure described in previous works [53,54]. The elastomer was first mixed with the corresponding curing agent at a 10:1 weight ratio. After manual mixing, the mixture was degassed in a desiccator for 30 min to remove air bubbles before proceeding with deposition.

Regarding the preparation of the cellulose derivatives, a 3 wt.% CMC solution was prepared by mixing the appropriate amount of the polymer with deionized water, which was kept under stirring for 24 h to yield a homogeneous gel. The EC matrix was produced by mixing 5 wt.% EC with a 50:50 mixture of ethanol and 4-hydroxy-4-methyl-2-pentanone with magnetic stirring for 24 h.

For the nanocomposites, hydrothermally synthesized ZnO nanorods were incorporated into a CMC matrix (ZnO@CMC) or an EC matrix (ZnO@EC) at a previously optimized loading of 25 wt.%. This loading was selected based on prior studies on energy harvesters, in which ZnO rods' concentrations between 15 and 30 wt.% were evaluated for ZnO particles dispersed in a PDMS polymeric matrix, with 25 wt.% yielding the highest output voltage [53,55]. The ZnO-polymer mixtures were magnetically stirred for at least 24 h to obtain homogeneous blends.

2.3. Fabrication of the Energy Harvesting Devices

Commercial indium tin oxide-coated PET (PET/ITO) substrates (Kintec Company, Kowloon, Hong Kong) with a resistivity of 60 $\Omega \cdot sq^{-1}$ were used as electrodes and substrates to produce EHDs. Two types of paper substrates were investigated as alternatives to the PET substrate: Whatman grade 1 chromatography paper (Whatman International Ltd., Florham Park, NJ, USA), characterized by its high porosity and Navigator standard paper (120 $g \cdot m^{-2}$, The Navigator Company, Lisbon, Portugal), a low-porosity paper with a whitening treatment.

The fabrication of the EHDs is illustrated in Figure 1. Film deposition was performed on one side of the PET/ITO or paper substrates using a K Control Coater (RK Print Coat Instruments, Royston, UK) with a wound metal bar (K101 Bar No. 8 Blue/100 Micron). Films with 100 µm wet thickness were produced, using a speed of 2 (approximately 0.6 $m \cdot min^{-1}$). The deposited films were subsequently dried at 60 °C for 3 h. Polyimide tape (DuPont, Delaware, USA) was used to assemble the electrodes on each side of the active layer and copper tape (3M, Minnesota, USA) was placed on each electrode to facilitate the connection between the devices and the oscilloscope used to evaluate their performance.

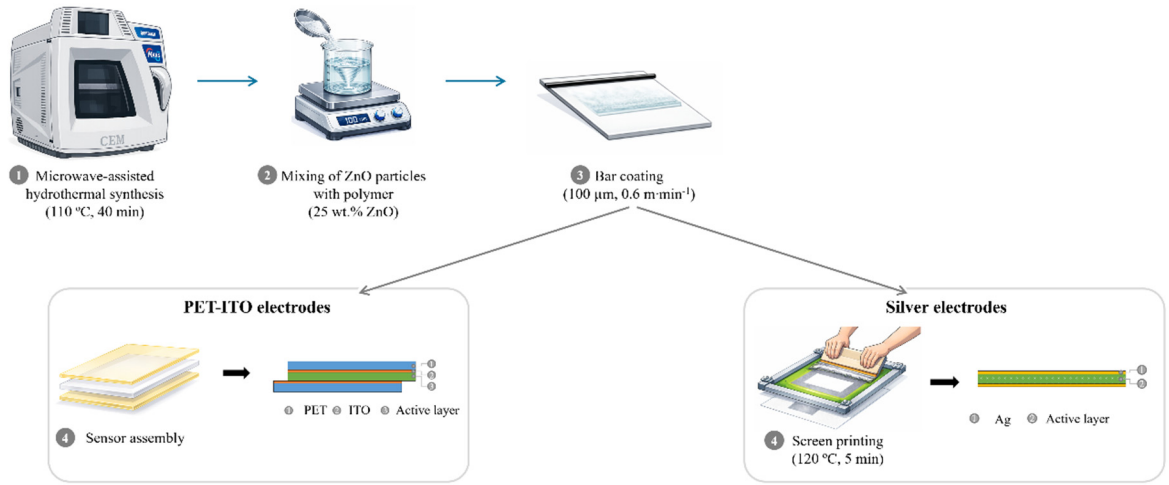

Figure 1. Schematic representation of the fabrication approaches used to produce the two types of EHDs, both incorporating a 100 µm active layer, using either PET/ITO electrodes or screen-printed silver electrodes on each side of a paper substrate. Image generated using ChatGPT (OpenAI, GPT-5.3) from prompts written by the author.

EHDs comprising a paper-based active layer sandwiched between screen-printed silver electrodes were also produced, as presented in Figure 1. First, the paper substrates were subjected to an ultraviolet/ozone (UV/O_3) treatment to improve the adhesion of the silver ink to their surface. The UV/O_3 treatment was performed for 5 min at room temperature using a PSD Pro Heated Series, PSDP-UVT Novascan system with emission wavelengths of 253.7 (90%) and 184.9 nm (10%) from Novascan Tech Inc. (Ames, IA, USA). Then, using a 120 T mesh with a (2 × 4) cm^2 rectangular pattern, conductive electrodes were printed on each side of the paper substrates. The electrodes were printed using the silver ink CRSN2442 from Suntronics (Sunchemical group, Parsippany-Troy Hills, NJ, USA) and cured at 120 °C for 5 min on a hot plate.

Different active layers were tested in each configuration, as summarized in Table 1, along with other critical experimental parameters for the production of the EHDs.

Table 1. Summary of critical experimental parameters for the EHDs produced herein.

Parameter	Value/Range
Substrate	None, Navigator paper (120 g·m^{-2}), Whatman paper
Polymeric matrix	None, PDMS, CMC (3 wt.%), EC (5 wt.%)
Deposition method	Bar coating (100 µm, 0.6 m·min^{-1})
Coating thickness	100 µm
ZnO loading concentration	0 wt.%, 25 wt.%
Electrodes	ITO on PET substrates, screen-printed silver
Active layer	Polymeric matrices (PDMS, CMC or EC) or Composites (ZnO@CMC or ZnO@EC) or Paper substrates (Navigator or Whatman) or Paper substrates embedded with matrices (Navigator or Whatman, with PDMS, CMC or EC) or Paper substrates embedded with composites (Navigator or Whatman, with ZnO@CMC or ZnO@EC)

The morphological properties of the hydrothermally synthesized ZnO structures and EHDs were analysed by scanning electron microscopy (SEM) using a TM3030Plus instrument (Hitachi, Tokyo, Japan). Images were acquired in a mode combining signals from both secondary and backscattered electron detectors, with an acceleration voltage of 15 kV. The dimensions of the ZnO rods (length and width) and the thickness of the paper-based active layers were determined from SEM images with the ImageJ software (version 1.53k). In addition, X-ray diffraction (XRD) patterns of the ZnO rods were collected with a Malvern Panalytical X'Pert PRO MRD diffractometer (Almelo, the Netherlands) equipped with Cu Kα radiation (λ = 1.540598 Å). Data were collected over a 2θ range of 20° to 80°, with a step size of 0.033° and a counting time of 35 s.

Zeta potential and conductivity measurements of 3 wt.% CMC and 5 wt.% EC solutions were performed using an Anton Paar (Graz, Austria) Litesizer 701 instrument. Measurements were conducted at a controlled temperature of 25 °C. Each sample was measured at least two times, and the reported values correspond to the average of these measurements.

Capacitance measurements were performed using a Keysight (Keysight Technologies, Santa Rosa, CA, USA) and a Cascade Microtech EPS 150 probe station (Cascade Microtech, Beaverton, OR, USA).

2.4. Electrical Characterization of the Devices

A home-made setup featuring a linear motor, similar to the one described by Rovisco et al. [54], was used to generate periodic mechanical stimulus. The stimulus was applied at a frequency of 1 Hz, with an impact area of 0.3 cm^2 and the applied force was estimated to be approximately 10 N, using a commercial force-sensing resistor (Ref. SEN05003, Interlink Electronics, Camarillo, CA, USA). The output voltage of the EHDs was measured with a digital 50 MHz bandwidth oscilloscope (TBS1000C, Tektronix, Beaverton, OR, USA) and 10 MΩ impedance probes (10× voltage probe, TPP0100, Tektronix).

To estimate the power density and perform the stability study of the best-performing devices, a force of 30 N at a frequency of 2 Hz was applied using a homemade setup that generated cyclic compressions (impact area of 5 cm^2). The output voltage to estimate the power density was measured across external load resistances ranging from 1 and 110 MΩ.

Data processing and statistical evaluation were performed in RStudio (version 2023.03.1). Group comparisons were analysed using Dunn's test, with a significance threshold set at a p-value of 0.05 or lower.

3. Results and Discussion

3.1. Morphological Characterization of the ZnO Rods

The ZnO rods produced herein by microwave-assisted hydrothermal synthesis were analyzed through XRD and SEM to assess their crystallinity, morphology and average size. The XRD diffractogram of the synthesized particles is presented in Figure 2a. The observed diffraction peaks are consistent with those reported in the ZnO reference card (ICDD card #36-1451). In particular, the peaks at 31.8°, 34.4°, 36.3° and 56.6° are assigned to the (100), (002), (101) and (110) lattice planes of the piezoelectric hexagonal wurtzite ZnO structure [56–58].

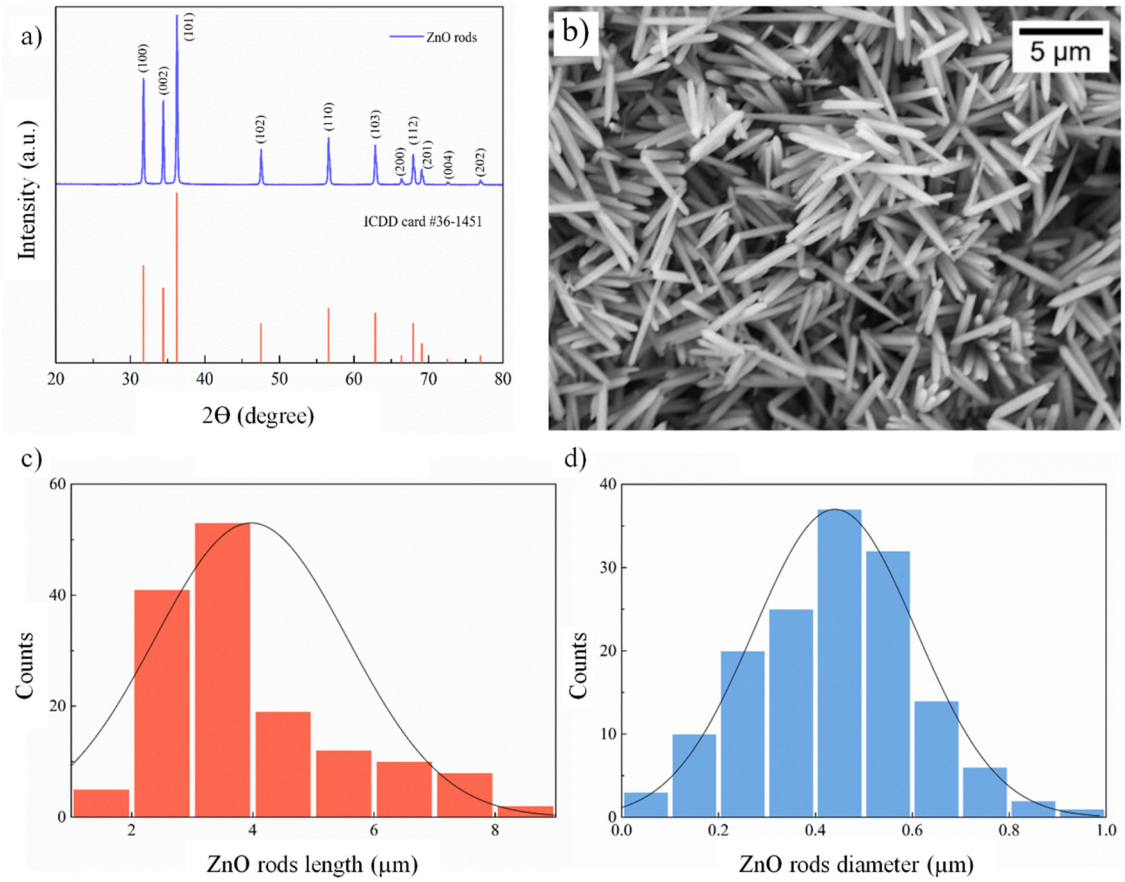

Figure 2. (**a**) XRD pattern, (**b**) SEM image and (**c**) length and (**d**) diameter histograms of the hydrothermally synthesized ZnO rods. The results presented in (**c**,**d**) are based on a total count of 150 rods obtained using ImageJ software. The black line shows the result of a Gaussian line fitting applied to the data.

Figure 2b presents an SEM image of the hydrothermally synthesized ZnO rods. It is possible to see that some ZnO particles are aggregated, which might be related to energetic principles [59,60]. The distributions of the ZnO rod's length and diameter values are displayed in Figure 2c,d. The distributions are approximately normal in both dimensions, as indicated by the Gaussian line-fitting of the data. The average length of the ZnO rods is (3.97 ± 1.59) µm, while the average diameter is (440 ± 168) nm, yielding an aspect ratio of approximately 9.

3.2. Morphological Characterization of the Papers and Papers with Embedded Matrices or Composites

Both the surface and cross-section topography of the paper substrates, either with or without an embedded matrix, were investigated through SEM images, as shown in Figure 3.

Figure 3a,i present the Whatman paper without an embedded matrix, demonstrating its high porosity due to the entangled fibers spaced apart and slightly loose, which leads to a high permeability [61]. In contrast, Figure 3e,m show Navigator paper without an embedded matrix, with evenly spread dots visible across the fiber surface. These dots are probably calcium carbonate, which is added to the paper during its production, serving as a filler that covers pores, a whitening agent and a surface-smoother [62–64]. As a result, the fibers are more tightly packed, reducing the space between them. This leads to lower porosity and permeability compared to Whatman paper [65]. When embedded with CMC, both papers show slightly more connections between the fibers, which is promoted by the dried CMC, as depicted in Figure 3b,f,j,n. In turn, upon embedding EC, both papers appear to become more compact, as shown in Figure 3c,g,k,o. Due to PDMS's higher viscosity compared to CMC and EC, PDMS was significantly less embedded in both papers than the cellulose derivatives. As a result, the top view of the papers with PDMS, Figure 3d,h, shows a concentrated polymeric layer, particularly on the deposition side of each substrate. These observations are supported by the cross-section images presented in Figure 3l,p, where a distinctive PDMS layer is evident atop both papers.

Figure 3q presents the average thickness values and standard deviations for papers with or without an embedded matrix. Notably, a significant distinction emerges between the standard deviation values of Navigator papers and those of Whatman papers. Navigator papers exhibit an average error (the ratio between the standard deviation and the respective average) of 2%, in contrast to the 6 % seen in Whatman papers. This suggests

Navigator's thickness is notably more consistent than Whatman's. A subtle reduction in thickness is observable when comparing the paper without an embedded matrix (control paper substrate) to the papers with embedded cellulose. For the Whatman paper, incorporation of cellulose derivatives resulted in an average thickness decrease of 13 µm (for EC) or 8 µm (for CMC). In contrast, for the Navigator paper, the reduction averaged 6 µm (for EC) and 5 µm (for CMC). This is supported by the SEM images, Figure 3c,g,k,o, where papers embedded with EC appear more compact. Moreover, Whatman paper samples experienced a more pronounced thickness reduction, likely due to their higher porosity and, consequently, a greater potential for pore reduction. Additionally, cellulose derivatives were more readily embedded in Whatman paper, leading to a higher amount of CMC or EC within the paper during drying, thereby inducing fiber contraction. Conversely, pristine Navigator paper already presents low porosity, affording less room for pore reduction upon the introduction of cellulose derivatives. When comparing the control papers with those containing PDMS as matrix, there is an increase in thickness from (133 ± 10) µm and (141 ± 2) µm to (153 ± 6) µm and (155 ± 2) µm for Whatman and Navigator papers. This reaffirms the earlier findings from the cross-section SEM images, Figure 3l,p, underscoring that PDMS did not penetrate as effectively into the papers as the cellulose derivatives did. Instead, the elastomer formed a top layer, augmenting the final thickness of the samples.

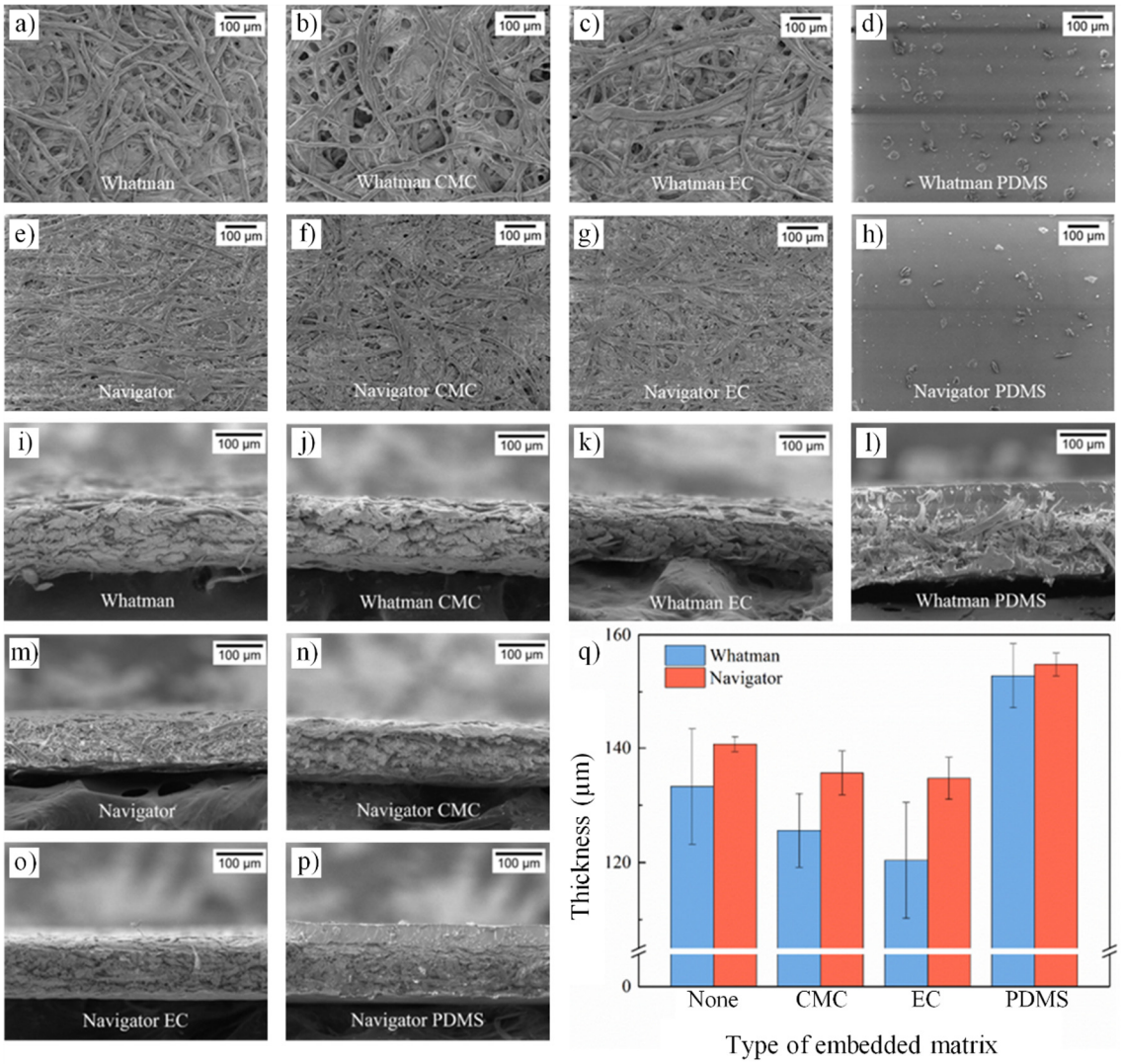

Figure 3. Morphological characterization of the paper-based active layers used to produce EHDs. (**a**–**h**) SEM surface images. (**i**–**p**) Cross-section images. (**q**) Thickness of the papers with or without an embedded matrix. Each column corresponds to an average of 10 measurements, and the error bars represent the corresponding standard deviation.

Regarding the nanocomposites, Supplementary Figure S1 presents images of the composites ZnO@CMC and ZnO@EC embedded in Whatman and Navigator papers, as well as these composites deposited onto PET/ITO substrates. Additionally, SEM analysis was performed on the paper substrates embedded with the composites to evaluate the dispersion of the ZnO particles in the cellulose derivatives matrix, and the obtained images are presented in Figure 4.

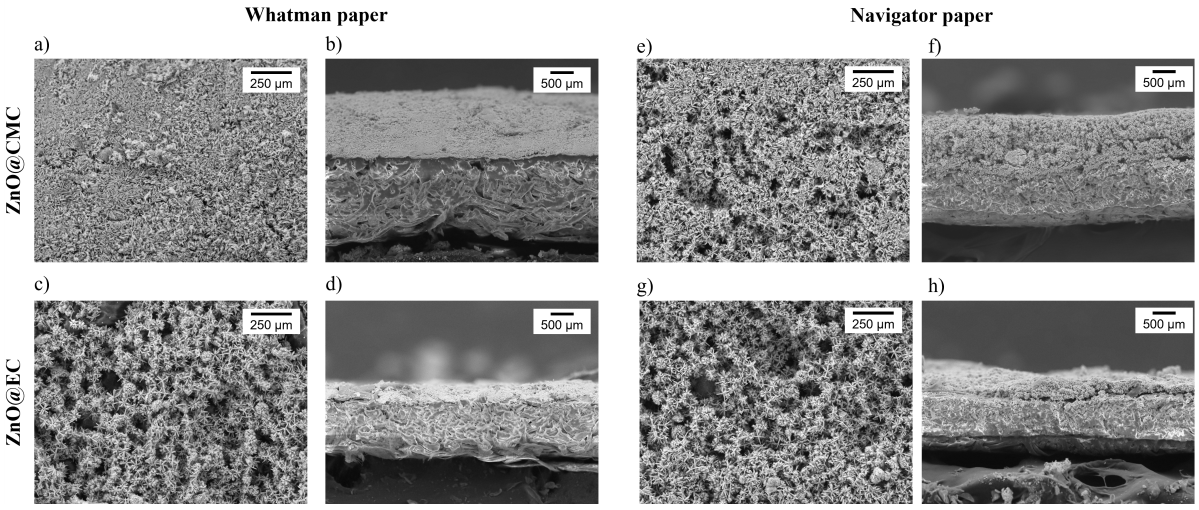

Figure 4. SEM images of the surface and cross-section of Whatman (**a**–**d**) and Navigator paper (**e**–**h**) substrates embedded with ZnO@CMC and ZnO@EC composites.

The SEM images reveal that the ZnO rods are more homogeneously dispersed within the CMC matrix (Figure 4a,e), leading to a more uniform coverage of the paper substrates. In contrast, the ZnO@EC coatings on both papers (Figure 4c,g) exhibit noticeable gaps, which may be attributed to the aggregates present in the corresponding mixtures. The dispersion of ZnO rods within the polymer matrix dictates the density and distribution of interfacial regions between the metal oxide particles and the polymer. These interfaces strongly influence charge trapping, separation and transport [66]. Particularly, particle agglomerates have been reported to act as pathways for charge transfer, providing more contact points with the polymeric matrix [66]. Cross-sectional images further reveal that the composites are more uniformly embedded within the Whatman paper substrates (Figure 4b,d), likely due to its higher porosity. Conversely, in the Navigator paper substrates the composites predominantly form a surface coating rather than penetrating the fiber network (Figure 4f,h).

3.3. Electrical Characterization of Devices with PET/ITO Electrodes

As an initial step, multiple EHDs were manufactured using PET/ITO substrates to establish a baseline for comparison with the additively manufactured EHDs. In these devices, the active layer comprised either the polymeric matrix alone (CMC, EC or PDMS) or a paper substrate with or without an embedded matrix. Figure 5 illustrates the output peak-to-peak voltage of these devices. As the piezoelectric structures were absent, the observed device output was attributed solely to the triboelectric effect at the interface between the active layer and the electrodes.

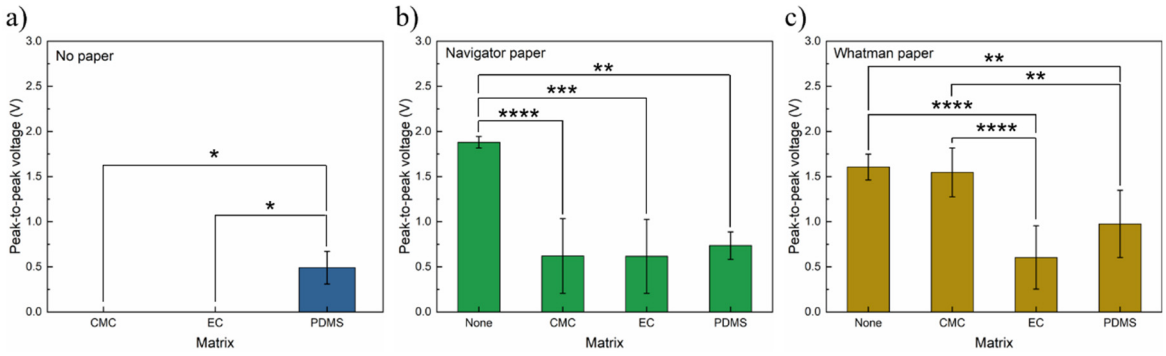

Figure 5. Peak-to-peak voltage response of EHDs featuring ITO electrodes in the absence of piezoelectric structures. (**a**) No paper, only matrix (CMC, EC and PDMS). (**b**) Navigator paper containing an embedded matrix (no matrix, CMC, EC, and PDMS). (**c**) Whatman paper with embedded matrix (no matrix, CMC, EC and PDMS). The significance levels are indicated by the number of stars as follows: * for p-value ≤ 0.05, ** for p-value ≤ 0.01, *** for p-value ≤ 0.001, and **** for p-value ≤ 0.0001.

In the case of devices with only a cellulosic-derivative polymeric matrix (CMC or EC) between the electrodes, as depicted in Figure 5a, no observable output is evident for each EHD type. This observation likely

arises from electrode short-circuiting caused by the thin cellulosic layers deposited on top of the ITO electrodes. In contrast, using PDMS as the active layer yields an average peak-to-peak voltage of around (0.49 ± 0.19) V. Thus, these results validate the proposed bar coating process as a scalable process to produce polymer-based EHDs.

Incorporating paper into the active layer resulted in higher peak-to-peak voltage values compared to devices containing only a polymeric matrix between the ITO electrodes, as indicated in Figure 5b,c, which can be ascribed to changes in the active layer thickness [67,68], roughness and higher compressibility [69–71]. Concerning devices using Navigator paper as the active layer, it is noteworthy that EHDs with just paper exhibit significantly greater output than those based on Navigator paper with a matrix (whether CMC, EC or PDMS), achieving a peak-to-peak voltage of (1.88 ± 0.06) V, with the difference being statistically significant. This higher output signal is associated with the more textured surface of the paper substrates, when devoid of embedded matrices, amplifying the triboelectric effect [72]. Furthermore, the fillers present in Navigator paper can also enhance this effect [73]. Regarding the cellulose derivatives-based EHDs, the preceding results (depicted in Figure 3) elucidate how the integration of the polymeric matrices into Navigator paper leads to denser paper and reduced thickness. Lower active layer thickness and surface area associated with lower capacity for compression through mechanical stimuli yielded smaller outputs, a phenomenon also observed in the literature [74,75].

In the case of EHDs with Whatman paper in the active layer, those without an embedded matrix exhibit comparable performance to those with an embedded CMC matrix, as depicted in Figure 5c, yielding outputs of (1.60 ± 0.14) V and (1.55 ± 0.27) V, respectively. The earlier findings (Figure 3) demonstrate that, with CMC, the thickness of the Whatman paper undergoes a slight reduction while porosity remains largely unaffected. Thus, the paper retains its porosity and surface roughness, facilitating the induction of triboelectric charges [76]. The CMC-based devices' performance significantly outperforms that of those based on EC or PDMS embedded in Whatman paper. EC notably reduces Whatman paper thickness, while PDMS imparts surface smoothing to the paper; both factors likely contribute to diminishing the triboelectric effect for the respective EHDs [75,77]. In addition to thickness-related effects, differences in EHD output can also be attributed to variations in the chemical structure of the cellulose derivatives. In particular, the presence of distinct functional groups introduced through cellulose derivatization, such as ester, carboxyl, or siloxane moieties, has been reported to influence the polymer's tendency to gain or lose electrons, thereby affecting its triboelectric behavior [71,78].

When comparing the peak-to-peak voltages of EHDs comprising each paper type, the highest value is obtained with Navigator paper without an embedded matrix as the active layer. As for the devices based on papers with an embedded matrix, EHDs with a CMC matrix embedded in Whatman paper exhibited notably higher output than those composed of Navigator paper with an embedded CMC, EC or PDMS matrix. These results indicate that PDMS could potentially be substituted by a cellulose-based matrix without substantial performance loss, or even with enhancement, as seen with CMC embedded in Whatman paper.

As the EHDs based on papers with CMC and EC presented performances comparable to that of PDMS-based devices, ZnO nanostructures were incorporated into these cellulose derivative mixtures and embedded into Whatman and Navigator paper. The goal was to enhance the devices' performance by combining the triboelectric effect, responsible for the results presented in Figure 5 with the improved performance associated with the incorporation of ZnO particles. The performance enhancement is attributed to (i) increased triboelectric charge generation associated with the high surface area of ZnO, (ii) charge trapping at the ZnO–polymer interfaces, and (iii) the intrinsic piezoelectric properties of this metal oxide [14,79]. To enable the comparison between devices with and without ZnO particles, the peak-to-peak voltage of devices based on cellulose-derivatives matrices (CMC or EC), either alone between the electrodes or incorporated into Navigator or Whatman paper, is presented again in Figure 6a. The peak-to-peak voltage of EHDs with active layers composed of either CMC or EC and ZnO composites sandwiched between PET/ITO electrodes or embedded into Navigator or Whatman paper is presented in Figure 6b.

In the devices with the polymeric cellulosic matrices sandwiched between the PET/ITO electrodes, the presence of ZnO significantly improved the output, as both CMC and EC-based devices showed an electrical response in the presence of ZnO, unlike what happened in its absence. The addition of ZnO to the matrices made the composite more viscous, resulting in a thicker layer and improved isolation of both electrodes, thereby preventing short-circuiting. It is worth noting that the output of EC-based devices increased twofold, revealing the fundamental role of ZnO in the EHDs response. This enhancement is attributed to the intrinsic piezoelectric properties of ZnO, together with its contribution to the triboelectric effect and charge trapping phenomena occurring at the ZnO–cellulose derivative interfaces [17,80].

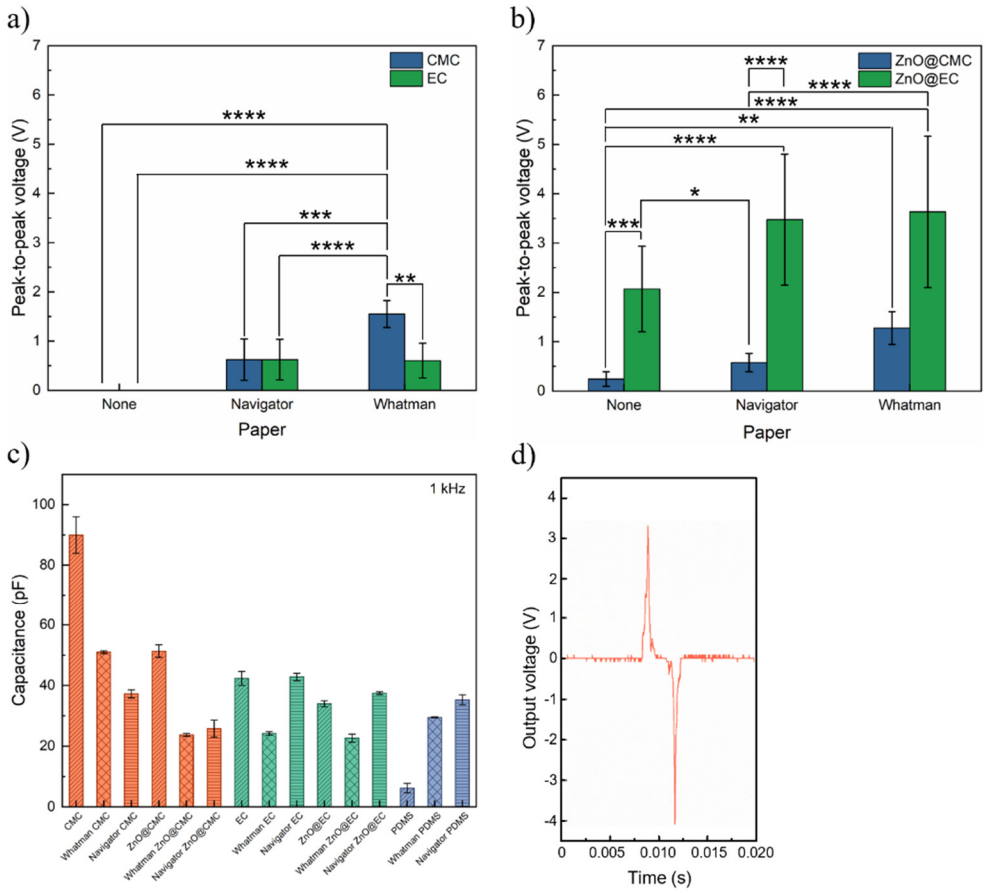

Figure 6. Output voltage values of EHDs with ITO electrodes, comparing configurations with and without ZnO particles. (**a**) EHDs without ZnO rods. (**b**) EHDs with ZnO rods. (**c**) Capacitance measurements of the different polymeric layers and corresponding composites. (**d**) Voltage output for the EHD with Whatman paper with embedded ZnO@EC. The significance levels are indicated by the number of stars as follows: * for p-value ≤ 0.05, ** for p-value ≤ 0.01, *** for p-value ≤ 0.001, and **** for p-value ≤ 0.0001.

Devices incorporating polymer-embedded Whatman or Navigator paper demonstrated a slight improvement in peak-to-peak voltage when compared to configurations without paper. In EHDs with Navigator paper with embedded CMC, the presence of ZnO rods did not seem to have a significant impact on the output. Conversely, the addition of ZnO to EC significantly improved the performance of the EHDs, as evidenced by peak-to-peak output voltage increases of 380% for Navigator-based devices and 454% for EHDs with Whatman paper.

Whatman and Navigator paper-based EHDs incorporating ZnO@EC composites exhibited higher peak-to-peak voltages than the devices based on ZnO@CMC composites, likely due to the anionic nature of CMC. To further investigate this effect, zeta potential measurements were performed on 3 wt.% CMC and 5 wt.% EC solutions. A zeta potential of (−42.65 ± 1.65) mV was obtained for CMC, whereas a value of (1.7 ± 0.2) mV was measured for EC. CMC is obtained by substituting hydroxyl groups on the cellulose backbone with carboxymethyl groups, which can ionize in solution to form negatively charged carboxylate groups. These negatively charged species, reflected in the measured zeta potential, may partially screen the piezoelectric charges generated during compression, thereby reducing the output voltage of the EHDs [71,78,81,82].

Additionally, the superior performance of the ZnO@EC devices may be related to the way the ZnO particles disperse within each matrix. These hydrothermally synthesized metal oxide particles are hydrophilic and therefore disperse more easily in CMC, which contains hydroxyl groups [83,84]. In EC, the ZnO particles do not disperse homogeneously and tend to form more aggregates, as evidenced by the SEM images of Figure 4c,g. This can also explain the higher decrease in capacitance values with the inclusion of ZnO for CMC devices (Figure 6c), for which capacitance was reduced to around half, when compared to EC-based devices, for which capacitance did not decrease nearly as much. CMC polymer chains strongly bind to the ZnO surface, forming a more rigid interfacial layer in which dipoles are not able to readily rotate under an electric field, thereby reducing polarization [85]. For EC, weak electrostatic interaction with ZnO leads to interfacial dipoles that can still respond to the electric field. Since lower capacitance is associated to higher voltage generation (for the same generated

charge), and the capacitance for devices with ZnO@CMC is comparable, and in some cases even lower, than for devices with EC (e.g., for Navigator paper), the lower voltage generation in ZnO@CMC seems be attributed to the charge screening taking place in CMC (large zeta potential), whereas for EC higher voltage outputs can be achieved. Without ZnO, the higher capacitance of CMC than EC, can be explained by their dielectric constant (5.3–5.7 [81] to 2–2.3 [86]), as the thickness is similar. In sum, the EHD with ITO electrodes with the best performance was based on ZnO@EC embedded on Whatman paper, with an average peak-to-peak voltage of (3.5 ± 0.8) V. An example of the output of such class of EHDs can be seen in Figure 6d, with a positive and negative peak clearly distinguishable, corresponding to the pushing and releasing, respectively. This class of EHDs could reach a peak-to-peak voltage of 7.4 V through finger tapping. For this device, the effective device d_{33} was estimated using Equation (1), which relates the generated charge and the applied force.

$$d_{33} = \frac{Q}{F} = \frac{C \cdot V}{F} \quad (1)$$

A value of $d_{33} = 0.6$ pC·N^{-1} was obtained, considering an average voltage amplitude of 3.5 V under an applied force of 10 N, and a capacitance of 1.65 pF corresponding to the 0.3 cm^2 area in which the stress is applied (the full device presented a capacitance of 22 pF over a 4 cm^2 area).

The effective piezoelectric coefficient is significantly lower than the intrinsic value for ZnO nanorods (~9 pC·N^{-1} [54]), which can be attributed to the low volumetric fraction of ZnO in the composite, the random orientation of the nanostructures and charge screening effects within the composite matrix.

3.4. Electrical Characterization of Devices with Silver Printed Electrodes

Pursuing the goal of producing functional and fully additively manufactured EHDs, silver electrodes were printed on both papers, Navigator and Whatman, and different combinations of said papers without an embedded matrix, with an embedded cellulose matrix (CMC or EC), or with embedded composites (ZnO@CMC, or ZnO@EC) were tested. The results are shown in Figure 7.

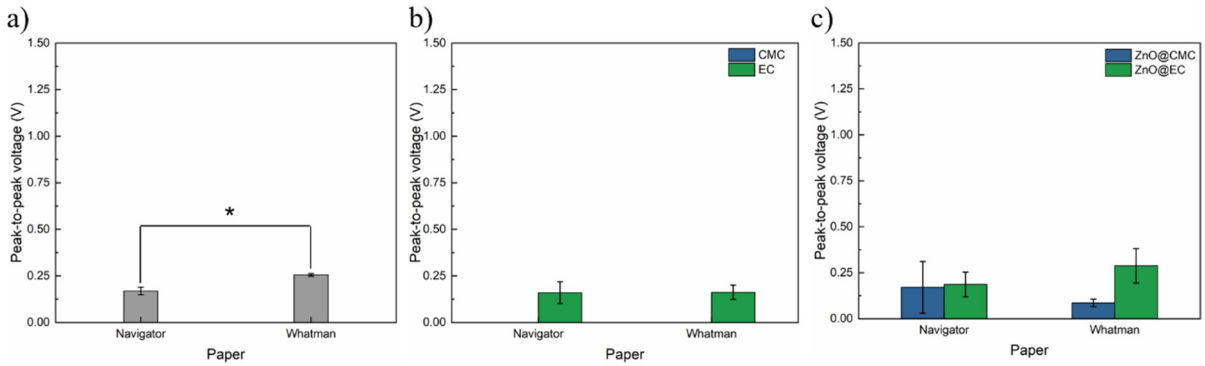

Figure 7. Output of the EHDs with printed silver electrodes (**a**) EHDs without an embedded matrix. (**b**) EHDs with embedded cellulose matrices. (**c**) EHDs with embedded composites. The significance levels are indicated by the number of stars as follows: * for *p*-value ≤ 0.05, ** for *p*-value ≤ 0.01, *** for *p*-value ≤ 0.001, and **** for *p*-value ≤ 0.0001.

EHDs with only paper exhibited small peak-to-peak voltages, between 0.08 V and 0.16 V. In the absence of piezoelectric structures in their composition, the output of these devices can be solely attributed to the triboelectric effect, which is limited since the electrodes are printed on both surfaces of the paper. The new EHD architecture limits the separation of the device's components during mechanical stimulation, resulting in low output [87,88]. Nevertheless, EHDs with Whatman paper presented a slightly higher output, which is attributed to this paper's higher porosity and, thus, greater ability to induce charges during compression [75,77].

Embedding the papers with EC produced no significant change in the output voltage compared to the EHDs composed of pristine counterparts and no significant differences were observed between EC embedded in Navigator or Whatman paper. In contrast, embedding either paper with CMC resulted in no detectable output signal. To further investigate whether this effect could be attributed to a low CMC coating thickness, EHDs were fabricated by coating a 200 µm CMC layer on both Whatman and Navigator paper and then screen-printing silver electrodes on each side of the substrates. However, no output signal was observed. As such, the absence of electrical output of the CMC/Ag devices may be attributed not just to the polymeric layer thickness but also to the conductivity of the CMC solution (4.138 mS·cm^{-1}), as determined from the zeta potential measurements, which is

significantly higher than that of the EC solution (0.025 $mS \cdot cm^{-1}$). Furthermore, the hygroscopic nature of CMC further promotes the ionic conductivity of the polymeric matrix [89,90]. The higher conductivity of the CMC system may promote charge leakage or screening effects, thereby preventing effective charge accumulation and reducing the measurable output signal.

Regarding the inclusion of ZnO particles, the addition of this metal oxide seems to have contributed to the performance enhancement, due to its piezoelectric properties, or the combination of both piezo and triboelectric phenomena [17,80]. There are no statistically significant differences between the two papers and the two types of ZnO composites. Nevertheless, the highest output among the cellulose derivatives-based EHDs was recorded for the configuration employing Whatman paper combined with ZnO@EC composites, which presented a peak-to-peak voltage value of (0.29 ± 0.01) V.

3.5. Stability and Electrical Output Performance of the ZnO@EC-Based Devices

Considering the results presented above, the EHDs based on Whatman and Navigator papers incorporating ZnO@EC composites and sandwiched between two PET/ITO electrodes were identified as the best-performing devices. To evaluate the long-term stability of these devices, 5000 continuous operating cycles, under an applied force of 30 N and 2 Hz, using a contact area of 5 cm^2, were recorded. As illustrated in Supplementary Figure S2, the nanogenerators maintained a generally stable performance even after exceeding 5000 cycles. The presented results highlight the stability of the ZnO@EC-based devices, as no significant changes in the output voltage are observed even after 5000 compression cycles, demonstrating their robustness and reliability. This behavior underscores the potential of these harvesters to operate continuously under repeated mechanical stimuli, which is essential for practical applications in energy harvesting and self-powered sensing systems.

To further assess the electrical performance of the harvesters, the voltage, current and power density generated by the ZnO@EC-based devices were evaluated as a function of load resistance (1 to 110 MΩ) under an applied force of 30 N, as shown in Figure 8.

The output voltage increases with increasing load resistance, whereas the current shows the opposite trend for both device types. In terms of power density, the Whatman ZnO@EC devices reach a maximum value of 0.25 $\mu W \cdot cm^{-2}$ at a load resistance of 22 MΩ. In contrast, devices based on ZnO@EC composites embedded in Navigator paper achieve a lower maximum power density of 0.045 $\mu W \cdot cm^{-2}$ at 10 MΩ. These findings further support previous observations, demonstrating that despite coating the substrates with the same ZnO@EC composite, device performance varies depending on the paper substrate, suggesting that differences in paper structure and composite integration influence the electromechanical response of the EHDs.

To better contextualize the performance of the developed devices, a comparison of representative ZnO-based nanogenerators reported in the literature, including the metal oxide synthesis process, device fabrication approaches and composing materials, as well as electrical output and power density values, is presented in Table 2.

Although the peak-to-peak voltage obtained for the two architectures tested is lower than those reported in the literature and still has room for improvement, the presented results pave the way for the development of more sustainable energy-harvesting devices. Regarding power density, the obtained values are lower than those reported in the literature, which can be attributed to the specific device architecture and operating conditions. It is also important to note that direct comparison between the devices listed in Table 2 is limited, as they were evaluated under different applied forces and device dimensions. Nevertheless, some general observations regarding device performance can still be drawn. In the tests performed with an active layer sandwiched between PET/ITO electrodes, the high output of paper-only devices was notable, due to the roughness of these materials [72,75]. However, Whatman, with embedded CMC presented an output voltage similar to the pristine paper, which was superior to the results obtained with PDMS. These results demonstrate the potential to replace this elastomer with more sustainable alternatives, such as cellulose derivatives or other nature-derived polymers. In addition, there was a significant increase in response upon inclusion of ZnO particles in the active layer, with peak-to-peak voltages equal to (3.5 ± 0.8) V being observed for devices based on ZnO@EC nanocomposites embedded in Whatman paper. Regarding EHDs based on paper substrates embedded in cellulose derivatives or nanocomposites with screen-printed electrodes, the obtained electrical output remains relatively low, highlighting the need to refine the harvester architecture and material interfaces. Furthermore, the development of multilayered devices should also be considered, as the use of different materials can enhance the triboelectric effect [88,91]. Still noteworthy are the additively manufactured EHDs with ZnO@EC nanocomposites, which exhibited a voltage of (0.29 ± 0.01) V, demonstrating the potential of these devices. Furthermore, the devices developed in this work offer several advantages, including simple and scalable fabrication process based on microwave-assisted hydrothermal synthesis and bar coating, as well as the incorporation of one-dimensional ZnO structures, which distinguishes

them from other reported devices and facilitates efficient integration into paper-based substrates. This approach provides a viable route toward multifunctional, eco-friendly paper-based platforms for flexible electronics that integrate energy harvesting, sensing, actuation, and electronic interfacing, with paper serving as both substrate and active layer.

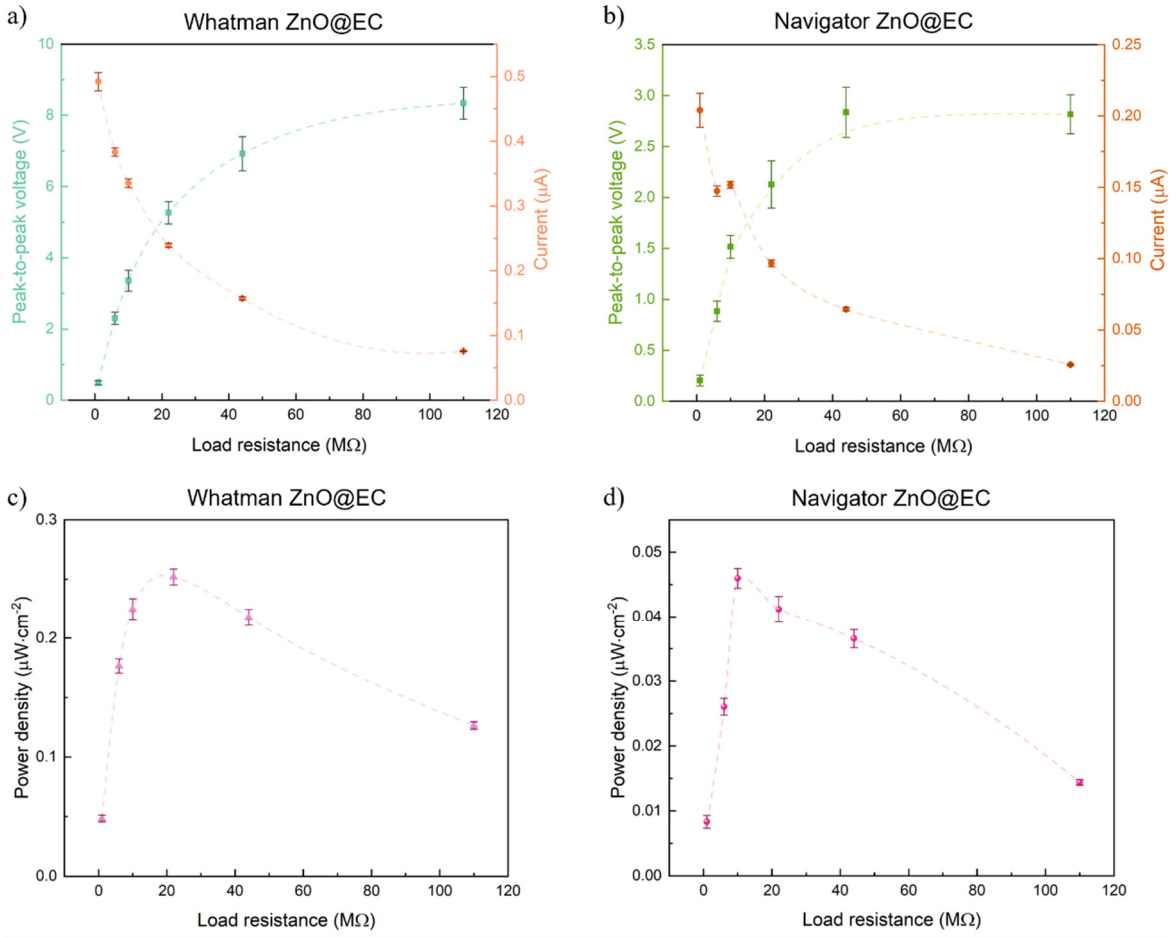

Figure 8. Peak-to-peak voltage and current (**a**,**b**) and power density (**c**,**d**) as a function of load resistance.

Table 2. Comparison of ZnO-based nanogenerators reported in the literature, including ZnO morphology and loading, synthesis method, device fabrication process and composing materials, voltage, and power density.

ZnO (Shape and Loading)	ZnO Synthesis Process	Active Layer Polymer	Substrate	Device Production Process	Voltage	Power Density	Ref.
Nanoparticles	Hydrothermal method	CRC	CRC, PDMS (encapsulation)	One-pot method	10 V (60 N)	0.731 μW·cm^{-2}	[92]
Nanoparticles (5 wt.%)	N/A (purchased)	CA	CA, ecoflex	Casting method	282.8 V	60 μW·cm^{-2}	[13]
Nanoparticles (0.1 g)	Sol-gel	HPMC	HPMC, PTFE	Spin coating	39.8 V	23 μW·cm^{-2}	[14]
Nanoparticles	Two-step hydrothermal process	CNF	CNF, PDMS	Two-step hydrothermal process, freeze-drying	25.6 V	-	[47]
Nanoparticles	Two-step hydrothermal process	CNF	PVDF	Electrospinning	11.8 V (45 N)	156 μW·cm^{-2}	[93]
Nanoparticles	N/A (purchased)	Bacterial cellulose	Bacterial cellulose, PET (encapsulation)	Physical blending	0.10V (0.5 N)	-	[6]
Nanoparticles	One-step hydrothermal process	CNF (3 wt.%)	CNF, polyamide tape (encapsulation)	One-step hydrothermal and self-assembly	5.61 V (50 N)	-	[94]
One- and two-dimensional nanoparticles	One-step hydrothermal method	C-MWCNTs /CNFs (2 wt. %)	PVDF	Electrospinning	19.5 V	2.62 μW·cm^{-2}	[95]
Rods (25 wt.%)	Microwave-assisted synthesis	EC (5 wt.%)	Whatman paper	Bar coating	3.5 V (10 N)	0.25 μW·cm^{-2}	This work
Rods (25 wt.%)	Microwave-assisted synthesis	EC (5 wt.%)	Navigator paper	Bar coating	3.4 V (10 N)	0.045 μW·cm^{-2}	This work

CRC: Cross-linked regenerated cellulose, CA: Cellulose acetate, HPMC: Hydroxypropyl methylcellulose, PTFE: Polytetrafluoroethylene, CNF: Cellulose nanofibril, C-MWCNTs: Carboxyl-functionalized multi-walled carbon nanotubes.

4. Conclusions

A sustainable approach for the development of piezoelectric energy harvesters was proposed. Devices with two architectures were developed using paper as the active layer; namely, one architecture was based on an active layer sandwiched between indium tin oxide-coated polyethylene terephthalate (PET/ITO) electrodes, whereas the other relied on conductive electrodes being screen printed on both sides of this layer. The performance of devices comprising only paper substrates (Whatman and Navigator) and paper substrates embedded with cellulose derivatives was studied and compared to that of devices with paper embedded with the commonly used polydimethylsiloxane (PDMS). Paper substrates yielded high peak-to-peak voltages derived from their rough surfaces. Embedding Whatman paper with cellulose derivatives, namely carboxymethyl cellulose, led to an output voltage of (1.55 ± 0.27) V, which was comparable to that of PDMS, (1.60 ± 0.14) V, highlighting the possibility of replacing this petroleum-derived polymer with more sustainable materials. The incorporation of hydrothermally synthesized zinc oxide (ZnO) particles was essential to improve the performance of the harvesters, with a maximum peak-to-peak voltage, under an impact force of 10 N of (3.5 ± 0.8) V being achieved with the Whatman paper embedded with ZnO/ethylcellulose composites sandwiched between PET/ITO electrodes. Regarding the devices produced by additive manufacturing, the same active layer yielded an output voltage of (0.29 ± 0.01) V. These results indicate that the tested materials can be incorporated into a layered device in order to increase the final peak-to-peak voltage of the energy harvester. This device can then be easily integrated into a paper-based multifunctional platform, supporting the development of greener electronics.

Supplementary Materials

The additional data and information can be downloaded at: https://media.sciltp.com/articles/others/2603310852389425/NC-26010026-SM.pdf. Figure S1. Images of the (2 × 2) cm^2 substrates with embedded composites explored to produce EHDs. Whatman paper embedded with (a) ZnO@CMC and (b) ZnO@EC. Navigator paper with embedded (c) ZnO@CMC and (d) ZnO@EC. PET/ITO substrate with (e) ZnO@CMC and (f) ZnO@EC. Figure S2. Output voltage of devices based on ZnO@EC composites embedded in (a) Whatman and (b) Navigator paper substrates over 5000 compression cycles at 30 N and 2 Hz (area = 5 cm^2).

Author Contributions

Conceptualization: A.R., A.d.S.; Methodology: T.S., C.G. and M.M.; Formal analysis and investigation: T.S., M.A. J.M.; Writing—original draft preparation: A.d.S., M.M.; Writing—review and editing: A.d.S., A.R., M. A. J.M., C.G., E.F., L.P., M.M., P.B., and R.M.; Funding acquisition: A.R., P.B., E.F., and R.M.; Resources: P.B., E.F. and R.M.; Supervision: A.d.S. and A.R. All authors have read and agreed to the published version of the manuscript.

Funding

This work was financed by national funds from FCT—Fundação para a Ciência e a Tecnologia, I.P., in the scope of the projects LA/P/0037/2020, UIDP/50025/2020 and UIDB/50025/2020 of the Associate Laboratory Institute of Nanostructures, Nanomodelling and Nanofabrication—i3N and the project FOLOW (2023.11887.PEX). M. Morais acknowledges funding from FCT, through the PhD Grant 2022.13806.BD (https://doi.org/10.54499/2022.13806.BD). This work was also funded by the European Union's Horizon 2020 Research and Innovation Programme under the EMERGE project (No. 101008701).

Institutional Review Board Statement

Not applicable.

Informed Consent Statement

Not applicable.

Data Availability Statement

Part of the datasets supporting the results of this study is described in the MSc thesis by Tiago Silva, entitled "*Sustainable Energy Harvesting Paper for Interactive Smart Packaging*". The thesis is available in the RUN institutional repository of NOVA University Lisbon and can be accessed at: http://hdl.handle.net/10362/147264 (accessed on 6 January 2026). Additional data supporting the findings of this manuscript can be obtained from the corresponding author upon reasonable request.

Conflicts of Interest

The authors declare no conflict of interest.

Use of AI and AI-Assisted Technologies

During the preparation of this work, the authors used ChatGPT (OpenAI, GPT-5.3) to generate one figure based on prompts written by the authors. After using this tool, the authors reviewed and edited the content as needed and take full responsibility for the content of the published article.

References

1. Silva, R.R.A.; Fatti, G.; Carlos, E.; et al. Functional Materials for Environmental Energy Harvesting in Smart Agriculture via Triboelectric Nanogenerators. *Adv. Funct. Mater.* **2026**, 36, e13924. https://doi.org/10.1002/adfm.202513924.
2. Chen, J.X.; Li, J.W.; Tsai, W.Y.; et al. High-performance piezoelectric flexible nanogenerators based on GO and polydopamine-modified ZnO/P(VDF–TrFE) for human motion energy capture, shared bicycle nanoenergy harvesting, and self-powered devices. *J. Colloid Interface Sci.* **2025**, *694*, 137666. https://doi.org/10.1016/j.jcis.2025.137666.
3. Xie, B.; Ma, Y.; Wang, J.; et al. Chemical Cross-Linking Cellulose Aerogel-Based Triboelectric Nanogenerators for Energy Harvesting and Sensing Human Activities. *ACS Appl. Mater. Interfaces* **2024**, *16*, 19411–19420. https://doi.org/10.1021/acsami.4c02671.
4. Qian, W.; Yang, Y. Cellulose-Templated Nanomaterials for Nanogenerators and Self-Powered Sensors. *Adv. Mater.* **2025**, *37*, 2412858. https://doi.org/10.1002/adma.202412858.
5. Gao, Z.; Zhou, Y.; Zhang, J.; et al. Advanced Energy Harvesters and Energy Storage for Powering Wearable and Implantable Medical Devices. *Adv. Mater.* **2024**, *36*, 2404492. https://doi.org/10.1002/adma.202404492.
6. Xiao, M.; Dong, X.; Wang, Z.; et al. Piezoelectric nanogenerators with bacterial cellulose-ZnO composites for human self-powered healthcare sensors. *J. Alloys Compd.* **2025**, *1032*, 181239. https://doi.org/10.1016/j.jallcom.2025.181239.
7. Lee, D.J.; Kumar, G.M.; Kim, D.Y.; et al. Highly Semiconducting One-Dimensional Porous ZnO Nanorod Array Nanogenerators for Mechanical Energy Harvesting Functions. *Int. J. Energy Res.* **2024**, *2024*, 5546570. https://doi.org/10.1155/2024/5546570.
8. Hussain, S.Z.; Singh, V.P.; Sadeque, M.S.B.; et al. Piezoelectric-Triboelectric Hybrid Nanogenerator for Energy Harvesting and Self-Powered Sensing Applications. *Small* **2025**, *21*, 2504626. https://doi.org/10.1002/smll.202504626.
9. Sezer, N.; Koç, M. A comprehensive review on the state-of-the-art of piezoelectric energy harvesting. *Nano Energy* **2021**, *80*, 105567. https://doi.org/10.1016/j.nanoen.2020.105567.
10. Sun, J.; Guo, H.; Ribera, J.; et al. Sustainable and Biodegradable Wood Sponge Piezoelectric Nanogenerator for Sensing and Energy Harvesting Applications. *ACS Nano* **2020**, *14*, 14665–14674. https://doi.org/10.1021/acsnano.0c05493.
11. Zou, Y.; Raveendran, V.; Chen, J. Wearable triboelectric nanogenerators for biomechanical energy harvesting. *Nano Energy* **2020**, *77*, 105303. https://doi.org/10.1016/j.nanoen.2020.105303.
12. Rasheed, A.; Ajmal, S.; Wang, P.; et al. Energizing the future: Unveiling challenges and prospects in MXene-based piezoelectric and triboelectric nanogenerators for micro- and nanoscale energy harvesting applications. *Appl. Mater. Today* **2024**, *39*, 102270. https://doi.org/10.1016/j.apmt.2024.102270.
13. Candido, I.C.M.; Freire, A.L.; Costa, C.A.R.; et al. Doped-Cellulose Acetate Membranes as Friction Layers for Triboelectric Nanogenerators: The Influence of Roughness Degree and Surface Potential on Electrical Performance. *Nanoenergy Adv.* **2024**, *4*, 196–209. https://doi.org/10.3390/nanoenergyadv4020012.
14. Baburaj, A.; Aliyana, A.K.; Kumar, S.K.N.; et al. High-performance biodegradable triboelectric nanogenerators based on hydroxypropyl methylcellulose and zinc oxide hybrid composites. *Nano Energy* **2024**, *128*, 109943. https://doi.org/10.1016/j.nanoen.2024.109943.
15. Pecunia, V.; Silva, S.R.P.; Phillips, J.D.; et al. Roadmap on energy harvesting materials. *J. Phys. Mater.* **2023**, *6*, 042501. https://doi.org/10.1088/2515-7639/acc550.
16. Jeong, J.; Jo, E.; Choi, J.A.; et al. Structural design strategies of triboelectric nanogenerators for omnidirectional wind energy harvesting. *Micro Nano Syst. Lett.* **2025**, *13*, 4. https://doi.org/10.1186/s40486-025-00224-6.
17. Zhao, S.; Han, G.; Deng, H.; et al. Polydimethylsiloxane-Zinc Oxide Nanorod-Based Triboelectric Nanogenerator for Compression Applications. *Materials* **2025**, *18*, 1392. https://doi.org/10.3390/ma18071392.
18. He, Q.; Briscoe, J. Piezoelectric Energy Harvester Technologies: Synthesis, Mechanisms, and Multifunctional Applications. *ACS Appl. Mater. Interfaces* **2024**, *16*, 29491–29520. https://doi.org/10.1021/acsami.3c17037.
19. Wang, Z.; Wang, Y.; Yang, C.; et al. Applications of Piezoelectric Materials in Biomedical Engineering. *Macromol. Biosci.* **2025**, *25*, 2500033. https://doi.org/10.1002/mabi.202500033.
20. Pan, X.; Wu, Y.; Wang, Y.; et al. Mechanical energy harvesting based on the piezoelectric materials: Recent advances and future perspectives. *Chem. Eng. J.* **2024**, *497*, 154249. https://doi.org/10.1016/j.cej.2024.154249.

21. Zhou, J.; Liu, M.; Gao, S.; et al. Design Strategies for High-Performance Piezoelectric Energy Harvesting Devices. *Adv. Mater.* **2025**, e12672. https://doi.org/10.1002/adma.202512672.
22. Nie, Z.; Kwak, J.W.; Han, M.; et al. Mechanically Active Materials and Devices for Bio-Interfaced Pressure Sensors—A Review. *Adv. Mater.* **2024**, *36*, 2205609. https://doi.org/10.1002/adma.202205609.
23. Zheng, Z.; Wang, X.; Hang, G.; et al. Recent progress on flexible poly(vinylidene fluoride)-based piezoelectric nanogenerators for energy harvesting and self-powered electronic applications. *Renew. Sustain. Energy Rev.* **2024**, *193*, 114285. https://doi.org/10.1016/j.rser.2024.114285.
24. Pierre Claver, U.; Zhao, G. Recent Progress in Flexible Pressure Sensors Based Electronic Skin. *Adv. Eng. Mater.* **2021**, *23*, 202001187. https://doi.org/10.1002/adem.202001187.
25. Chittibabu, S.K.; Chintagumpala, K.; Chandrasekhar, A. Porous dielectric materials based wearable capacitance pressure sensors for vital signs monitoring: A review. *Mater. Sci. Semicond. Process.* **2022**, *151*, 106976. https://doi.org/10.1016/j.mssp.2022.106976.
26. Shi, Z.; Meng, L.; Shi, X.; et al. Morphological Engineering of Sensing Materials for Flexible Pressure Sensors and Artificial Intelligence Applications. *Nano-Micro Lett.* **2022**, *14*, 141. https://doi.org/10.1007/s40820-022-00874-w.
27. Ghosh, R. Recent progress in piezotronic sensors based on one-dimensional zinc oxide nanostructures and its regularly ordered arrays: From design to application. *Nano Energy* **2023**, *113*, 108606. https://doi.org/10.1016/j.nanoen.2023.108606.
28. John, D.M.; Annamalai, P.K.; Hosseinmardi, A.; et al. Progress in Zinc Oxide-Based Polymer Nanocomposites for Advancing Piezoelectric Energy Harvesting and Self-Powered Devices. *Macromol. Mater. Eng.* **2025**, *310*, e00239. https://doi.org/10.1002/mame.202500239.
29. Yang, D.; Sun, A.; Pan, Y.; et al. Mechanical energy harvesting: Advancements in piezoelectric nanogenerators. *Int. J. Electrochem. Sci.* **2024**, *19*, 100793. https://doi.org/10.1016/j.ijoes.2024.100793.
30. Hsieh, G.W.; Shih, L.C.; Chen, P.Y. Porous Polydimethylsiloxane Elastomer Hybrid with Zinc Oxide Nanowire for Wearable, Wide-Range, and Low Detection Limit Capacitive Pressure Sensor. *Nanomaterials* **2022**, *12*, 256. https://doi.org/10.3390/nano12020256.
31. Nikolaeva, A.V.; Kondratev, V.M.; Kadinskaya, S.A.; et al. ZnO nanowire-based flexible sensors for pressure and temperature monitoring. *Mater. Sci. Semicond. Process.* **2025**, *189*, 109253. https://doi.org/10.1016/j.mssp.2024.109253.
32. Moezzi, M.; Bakhtari, K.; Ranjbar-Mohammadi, M.; et al. Fabrication and characterization of piezoelectric poly (lactic acid)/ZnO bionanocomposite films. *Polym. Bull.* **2025**, *82*, 4423–4442. https://doi.org/10.1007/s00289-025-05706-6.
33. Jeronimo, K.; Koutsos, V.; Cheung, R.; et al. PDMS-ZnO Piezoelectric Nanocomposites for Pressure Sensors. *Sensors* **2021**, *21*, 5873. https://doi.org/10.3390/s21175873.
34. Sun, Y.; Liu, Y.; Zheng, Y.; et al. Enhanced Energy Harvesting Ability of ZnO/PAN Hybrid Piezoelectric Nanogenerators. ACS Appl. *Mater. Interfaces* **2020**, *12*, 54936–54945. https://doi.org/10.1021/acsami.0c14490.
35. Slimani Tlemcani, T.; Justeau, C.; Nadaud, K.; et al. Fabrication of Piezoelectric ZnO Nanowires Energy Harvester on Flexible Substrate Coated with Various Seed Layer Structures. *Nanomaterials* **2021**, *11*, 1433. https://doi.org/10.3390/nano11061433.
36. John, D.M.; Pillai, N.S.; Sivan, A.; et al. Ferromagnetic ZnO nanostructures from an organo zinc complex formulated via Piper Longum L-assisted green synthesis: Multifaceted prospects in photocatalysis, antimicrobial activity, and cell viability studies. *Heliyon* **2024**, *10*, e33360. https://doi.org/10.1016/j.heliyon.2024.e33360.
37. Saeeda Javaid, A.; Saeeda Javaid, W.; Adnan, M.; et al. Synthesis and characterization of efficient Sr-doped ZnO nanostructures for optoelectronic, and photocatalytic applications. *Inorg. Chem. Commun.* **2024**, *162*, 112175. https://doi.org/10.1016/j.inoche.2024.112175.
38. Lee, J.E.; Lim, C.K.; Park, H.J.; et al. ZnO–CuO Core-Hollow Cube Nanostructures for Highly Sensitive Acetone Gas Sensors at the ppb Level. ACS Appl. *Mater. Interfaces* **2020**, *12*, 35688–35697. https://doi.org/10.1021/acsami.0c08593.
39. Cunha, I.; Martins, J.; Bahubalindruni, P.G.; et al. Handwritten and Sustainable Electronic Logic Circuits with Fully Printed Paper Transistors. *Adv. Mater. Technol.* **2021**, *6*, 2100633. https://doi.org/10.1002/admt.202100633.
40. Carvalho, J.T.; Dubceac, V.; Grey, P.; et al. Fully printed zinc oxide electrolyte-gated transistors on paper. *Nanomaterials* **2019**, *9*, 169. https://doi.org/10.3390/nano9020169.
41. Grey, P.; Gaspar, D.; Cunha, I.; et al. Handwritten Oxide Electronics on Paper. *Adv. Mater. Technol.* **2017**, *2*, 170009. https://doi.org/10.1002/admt.201700009.
42. Ferreira, S.H.; Cunha, I.; Pinto, J.V.; et al. UV-Responsive Screen-Printed Porous ZnO Nanostructures on Office Paper for Sustainable and Foldable Electronics. *Chemosensors* **2021**, *9*, 192. https://doi.org/10.3390/chemosensors9080192.
43. Pinheiro, T.; Silvestre, S.; Coelho, J.; et al. Laser-Induced Graphene on Paper toward Efficient Fabrication of Flexible, Planar Electrodes for Electrochemical Sensing. *Adv. Mater. Interfaces* **2021**, *8*, 2101502. https://doi.org/10.1002/admi.202101502.
44. Chen, S.; Jiang, J.; Xu, F.; et al. Crepe cellulose paper and nitrocellulose membrane-based triboelectric nanogenerators for energy harvesting and self-powered human-machine interaction. *Nano Energy* **2019**, *61*, 69–77. https://doi.org/10.1016/j.nanoen.2019.04.043.

45. Wu, C.; Kim, T.W.; Sung, S.; et al. Ultrasoft and cuttable paper-based triboelectric nanogenerators for mechanical energy harvesting. *Nano Energy* **2018**, *44*, 279–287. https://doi.org/10.1016/j.nanoen.2017.11.080.
46. Xia, K.; Zhang, H.; Zhu, Z.; et al. Folding triboelectric nanogenerator on paper based on conductive ink and teflon tape. *Sens. Actuators A Phys.* **2018**, *272*, 28–32. https://doi.org/10.1016/j.sna.2018.01.054.
47. Song, X.; Zhuo, B.; Cao, S.; et al. High performance and flexible piezoelectric composite incorporating zinc oxide grown on the oxidized nanocellulose by two-step hydrothermal process. *Appl. Surf. Sci.* **2024**, *649*, 158996. https://doi.org/10.1016/j.apsusc.2023.158996.
48. Maiti, S.; Karan, S.K.; Kim, J.K.; et al. Nature Driven Bio-Piezoelectric/Triboelectric Nanogenerator as Next-Generation Green Energy Harvester for Smart and Pollution Free Society. *Adv. Energy Mater.* **2019**, 9, 1803027. https://doi.org/10.1002/aenm.201803027.
49. Li, J.; Long, Y.; Yang, F.; et al. Degradable piezoelectric biomaterials for wearable and implantable bioelectronics. *Curr. Opin. Solid State Mater. Sci.* **2020**, *24*, 100806. https://doi.org/10.1016/j.cossms.2020.100806.
50. Zheng, Q.; Zhang, H.; Mi, H.; et al. High-performance flexible piezoelectric nanogenerators consisting of porous cellulose nanofibril (CNF)/poly(dimethylsiloxane) (PDMS) aerogel films. *Nano Energy* **2016**, *26*, 504–512. https://doi.org/10.1016/j.nanoen.2016.06.009.
51. Alhazime, A.A. Improving the functional properties of chitosan/carboxymethyl cellulose biopolymer blend by incorporating zinc oxide/aluminium oxide nanofillers for advanced energy storage and optoelectronic applications. *Int. J. Biol. Macromol.* **2025**, *320*, 146083. https://doi.org/10.1016/j.ijbiomac.2025.146083.
52. Upadhye, P.A.; Chowdhury, S.R.; Kumar, V.; et al. Hollow ZnO nanorod in PVDF matrix for high-performance sensing, vibration energy harvesting and wearable application. *Sci. Rep.* **2025**, *15*, 19885. https://doi.org/10.1038/s41598-025-04577-1.
53. dos Santos, A.; Sabino, F.; Rovisco, A.; et al. Optimization of ZnO Nanorods Concentration in a Micro-Structured Polymeric Composite for Nanogenerators. *Chemosensors* **2021**, *9*, 27. https://doi.org/10.3390/chemosensors9020027.
54. Rovisco, A.; dos Santos, A.; Cramer, T.; et al. Piezoelectricity Enhancement of Nanogenerators Based on PDMS and $ZnSnO_3$ Nanowires through Microstructuration. *ACS Appl. Mater. Interfaces* **2020**, *12*, 18421–18430. https://doi.org/10.1021/acsami.9b21636.
55. Henriques Ferreira, S.; Rovisco, A.; dos Santos, A.; et al. *Porous ZnO Nanostructures Synthesized by Microwave Hydrothermal Method for Energy Harvesting Applications*; IntechOpen: London, UK, 2021. https://doi.org/10.5772/intechopen.97060.
56. Alshehri, N.A.; Lewis, A.R.; Pleydell-Pearce, C.; et al. Investigation of the growth parameters of hydrothermal ZnO nanowires for scale up applications. *J. Saudi Chem. Soc.* **2018**, *22*, 538–545. https://doi.org/10.1016/j.jscs.2017.09.004.
57. Ojha, D.P.; Joshi, B.; Samuel, E.; et al. Supersonically Sprayed Flexible ZnO/PVDF Composite Films with Enhanced Piezoelectricity for Energy Harvesting and Storage. *Int. J. Energy Res.* **2023**, *2023*, 3074782. https://doi.org/10.1155/2023/3074782.
58. Fakhri, P.; Eaianli, N.; Bagherzadeh, R.; et al. Sandwich-type double-layer piezoelectric nanogenerators based on one- and two-dimensional ZnO nanostructures with improved output performance. *Sci. Rep.* **2023**, *13*, 16412. https://doi.org/10.1038/s41598-023-43047-4.
59. Mohan Kumar, K.; Mandal, B.K.; Appala Naidu, E.; et al. Synthesis and characterisation of flower shaped Zinc Oxide nanostructures and its antimicrobial activity. *Spectrochim. Acta Part A Mol. Biomol. Spectrosc.* **2013**, *104*, 171–174. https://doi.org/10.1016/j.saa.2012.11.025.
60. Kołodziejczak-Radzimska, A.; Jesionowski, T. Zinc Oxide—From Synthesis to Application: A Review. *Materials* **2014**, *7*, 2833–2881. https://doi.org/10.3390/ma7042833.
61. Natarajan, S.; Jayaraj, J.; Prazeres, D.M.F. A Cellulose Paper-Based Fluorescent Lateral Flow Immunoassay for the Quantitative Detection of Cardiac Troponin I. *Biosensors* **2021**, *11*, 49. https://doi.org/10.3390/bios11020049.
62. Ilhan, V. *Soda Ash for Paper Industry*; PetroNaft Co Research Team: Ankara, Turkey, 2024.
63. Maślana, K.; Sielicki, K.; Wenelska, K.; et al. Facile Strategy for Boosting of Inorganic Fillers Retention in Paper. *Polymers* **2023**, *16*, 110. https://doi.org/10.3390/polym16010110.
64. Dhakad, V.K.; Shrivastava, P.; Agarwal, S.; et al. Synthesis and characterization of precipitated calcium carbonate from marble waste for its application in papermaking. Clean Technol. *Environ. Policy* **2024**, *26*, 3539–3556. https://doi.org/10.1007/s10098-024-02813-2.
65. Oliveira, M.J.; Quaresma, P.; Peixoto de Almeida, M.; et al. Office paper decorated with silver nanostars—An alternative cost effective platform for trace analyte detection by SERS. *Sci. Rep.* **2017**, *7*, 2480. https://doi.org/10.1038/s41598-017-02484-6.
66. Venkatesan, H.M.; Yoon, J.U.; Bindhu, A.; et al. High-performance triboelectric nanogenerators based on Ag-doped ZnO loaded electrospun PVDF nanofiber mats for energy harvesting and healthcare monitoring. *Sci. Rep.* **2025**, *15*, 3347. https://doi.org/10.1038/s41598-025-87148-8.

67. Zhang, Z.; Sun, X.; Chen, Y.; et al. Comprehensive dependence of triboelectric nanogenerator on dielectric thickness and external impact for high electric outputs. *J. Appl. Phys.* **2018**, *124*, 045106. https://doi.org/10.1063/1.5031809.
68. Song, W.Z.; Zhang, T.T.; Zhang, D.S.; et al. Highly stretchable conductors reveal the effect of dielectric layer thickness on triboelectric nanogenerator output. *Nano Energy* **2023**, *114*, 108621. https://doi.org/10.1016/j.nanoen.2023.108621.
69. Rajabi-Abhari, A.; Yoo, H.; Kim, J.; et al. Reversibly Compressible Silanated Cellulose Nanofibril Aerogel for Triboelectric Taekwondo Scoring Sensors. *Small* **2024**, *20*, 2405664. https://doi.org/10.1002/smll.202405664.
70. Sabu, A.; Nair, M.B.; et al. Morphology-driven multifunctionality: Tailoring ZnO for enhanced EMI shielding and energy harvesting in PVDF/MWCNT nanocomposites. *Nanoscale* **2025**, *17*, 23296–23314. https://doi.org/10.1039/D5NR03391H.
71. Du, G.; Wang, J.; Liu, Y.; et al. Fabrication of Advanced Cellulosic Triboelectric Materials via Dielectric Modulation. *Adv. Sci.* **2023**, *10*, 2206243. https://doi.org/10.1002/advs.202206243.
72. Kim, W.G.; Kim, D.W.; Tcho, I.W.; et al. Triboelectric Nanogenerator: Structure, Mechanism, and Applications. *ACS Nano* **2021**, *15*, 258–287. https://doi.org/10.1021/acsnano.0c09803.
73. Zhang, R.; Hummelgård, M.; Örtegren, J.; et al. Energy Harvesting Using Wastepaper-Based Triboelectric Nanogenerators. *Adv. Eng. Mater.* **2023**, *25*, 2300107. https://doi.org/10.1002/adem.202300107.
74. Yahyapour, R.; Sorayani Bafqi, M.S.; Latifi, M.; et al. Hybrid multilayered piezoelectric energy harvesters with non-piezoelectric layers. *J. Mater. Sci.: Mater. Electron.* **2022**, *33*, 1783–1797. https://doi.org/10.1007/s10854-021-07296-1.
75. Repoulias, A.; Logothetis, I.; Matsouka, D.; et al. Contact Area of Electrification Materials Relating to Triboelectric Generators: A Comparative Study. *Electron. Mater. Lett.* **2024**, *20*, 283–292. https://doi.org/10.1007/s13391-023-00470-z.
76. Zhang, R.; Chen, D.; Hummelgård, M.; et al. Engineering Triboelectric Paper for Energy Harvesting and Smart Sensing. *Adv. Mater.* **2025**, *37*, 2416641. https://doi.org/10.1002/adma.202416641.
77. Bakhtiyari, S.; Bagherzadeh, R.; Ezazshahabi, N.; et al. Yarn-to-Yarn Surface Area and Roughness as Structural Engineering Tools for Optimizing the Electrical Output of Triboelectric Nanogenerators: Geometrical and Experimental Verification. *Adv. Mater. Technol.* **2025**, *10*, 2401346. https://doi.org/10.1002/admt.202401346.
78. Zhou, J.; Wang, H.; Du, C.; et al. Cellulose for Sustainable Triboelectric Nanogenerators. *Adv. Energy Sustain. Res.* **2022**, *3*, 2100161. https://doi.org/10.1002/aesr.202100161.
79. Venkatesan, H.M.; Thandavan, K.; et al. Reinforcing the Strategy: Enhanced Efficiency of Electrospun PVDF Hybrid Nanocomposites-Based Triboelectric Nanogenerators with p-NiO/n-ZnO Interfaces for Energy Harvesting. *Adv. Sustain. Syst.* **2025**, *9*, e00180. https://doi.org/10.1002/adsu.202500180.
80. Lim, Y.P.; Zhao, J.; et al. Modulating ZnO Growth Structures for Maximum Power Output of Hybrid Piezo/Triboelectric Nanogenerator. *Adv. Funct. Mater.* **2022**, *32*, 2206750. https://doi.org/10.1002/adfm.202206750.
81. Gallegos-Rosas, K.; Azari, A.; Soldano, C. Carboxymethyl Cellulose as a Sustainable Dielectric Material for Organic Field-Effect Transistors. *ACS Appl. Electron. Mater.* **2025**, *7*, 1274–1282. https://doi.org/10.1021/acsaelm.4c02227.
82. Zou, H.; Zhang, Y.; Guo, L.; et al. Quantifying the triboelectric series. *Nat. Commun.* **2019**, *10*, 1427. https://doi.org/10.1038/s41467-019-09461-x.
83. Rai, R.S. Development of hydrophilic carbon fiber textiles using seed-assisted hydrothermal deposition of ZnO nanostructures for enhanced interfacial interaction in CFRP composites. *Ceram. Int.* **2024**, *50*, 52871–52880. https://doi.org/10.1016/j.ceramint.2024.10.139.
84. Nundy, S.; Ghosh, A.; Mallick, T.K. Hydrophilic and Superhydrophilic Self-Cleaning Coatings by Morphologically Varying ZnO Microstructures for Photovoltaic and Glazing Applications. *ACS Omega* **2020**, *5*, 1033–1039. https://doi.org/10.1021/acsomega.9b02758.
85. Al-Rafai, H.; Khalil, K.D.; Bashal, A.H.; et al. Revolutionizing dielectric and electrical properties of carboxymethylcellulose/ZnO nanocomposites: A detailed exploration of experimental findings and computational insights for advanced material engineering. *Int. J. Biol. Macromol.* **2025**, *308*, 142406. https://doi.org/10.1016/j.ijbiomac.2025.142406.
86. Niu, F.; Song, R.; Rong, Y.; et al. One-Step Preparation of Ethyl Cellulose Films with Asymmetric Graded Pores for Low Dielectric Printing Substrates. *Adv. Mater.* **2026**, *38*, e07704. https://doi.org/10.1002/adma.202507704.
87. Keel, E.; Ejaz, A.; Mckinlay, M.; et al. Three-dimensional graphene foam based triboelectric nanogenerators for energy systems and autonomous sensors. *Nano Energy* **2023**, *112*, 108475. https://doi.org/10.1016/j.nanoen.2023.108475.
88. Li, C.; Bai, Y.; Shao, J.; et al. Strategies to Improve the Output Performance of Triboelectric Nanogenerators. *Small Methods* **2024**, *8*, 2301682. https://doi.org/10.1002/smtd.202301682.
89. Akhlaq, M.; Mushtaq, U.; Naz, S.; et al. Carboxymethyl cellulose-based materials as an alternative source for sustainable electrochemical devices: A review. *RSC Adv.* **2023**, *13*, 5723–5743. https://doi.org/10.1039/D2RA08244F.
90. Sabrina, Q.; Ratri, C.R.; Hardiansyah, A.; et al. Flexible fibrous structure of bacterial cellulose by synergic role carboxymethyl cellulose and glycerol for LiB polymer electrolyte. *Mater. Res. Express* **2023**, *10*, 055305. https://doi.org/10.1088/2053-1591/acd67c.
91. Ji, H.; Sun, C.; Sun, X.; et al. Perspectives of Material Optimization Strategies for High-Performance Triboelectric Nanogenerators. *Adv. Sustain. Syst.* **2024**, *8*, 2300583. https://doi.org/10.1002/adsu.202300583.

92. Song, X.; Zou, H.; Cao, S.; et al. Flexible regenerated cellulose/ZnO based piezoelectric composites fabricated via an efficient one-pot method to load high-volume ZnO with assistance of crosslinking. *Chem. Eng. J.* **2023**, *475*, 146184. https://doi.org/10.1016/j.cej.2023.146184.
93. Zhu, Q.; Song, X.; Chen, X.; et al. A high performance nanocellulose-PVDF based piezoelectric nanogenerator based on the highly active CNF@ZnO via electrospinning technology. *Nano Energy* **2024**, *127*, 109741. https://doi.org/10.1016/j.nanoen.2024.109741.
94. Chen, Q.; Song, X.; Xiao, L.; et al. Efficient and tight self-assembly from CNF@ZnO synthesized via an one-step hydrothermal method to fabricate cellulose based piezoelectric composite. *Ind. Crops Prod.* **2025**, *237*, 122007. https://doi.org/10.1016/j.indcrop.2025.122007.
95. Ma, J.; Song, X.; Xiao, L.; et al. C-MWCNTs/cellulose nanofibers dual-network substrate strategy improving the in-situ growth of ZnO for high-performance piezoelectric and sensing devices. *Chem. Eng. J.* **2026**, *528*, 172267. https://doi.org/10.1016/j.cej.2025.172267.